# Thermal design of cooling channels in an injection plastic mold by overset-based numerical optimization technique

Vincent Sobotka, Bruno Storti

# THERMAL DESIGN OF COOLING CHANNELS IN AN INJECTION PLASTIC MOLD BY OVERSET-BASED NUMERICAL OPTIMIZATION TECHNIQUE

**Bruno A. Storti[1*], Vincent Sobotka[1]**

[1]Nantes Université, CNRS, Laboratoire de thermique et énergie de Nantes, LTeN, UMR 6607, La Chantrerie, rue Christian Pauc, 44306 Nantes cedex 03, France

## ABSTRACT

Due to the change of standard on the actual manufacturing industry from mass production to a made-to-order perspective, injection mold (IM) manufacturers are often demanded for rapid tooling to deal with small batches and rapid prototyping. The additive manufacturing (AM) process accomplishes such requirements by producing polymer mold inserts quickly while saving costs, regardless of the complexity of the geometry. Despite the appeal of soft tooling, the life of such plastic-made additive IM inserts remains unclear, and numerous studies relate their early failure to non-suitable thermal regulation. Further, the low thermal diffusivity of commercial polymers usually employed on AM IM eventually leads to high cycle times and the uneven cooling of the injected material, affecting the final quality of the part. To cope with such drawbacks, a high-performance polymer conformed by a polycarbonate matrix charged with carbon fibers is formulated in this work to enhance the thermal conductivity of the tooling material. In addition, an accurate optimization methodology based on three-dimensional overset meshes in the finite element method context is introduced to find a suitable arrangement of curved cooling channels (CC) within the insert to improve the temperature uniformity of the injected part. A function involving two terms accounting for temperature standard deviation and maximum thermal gradients on the part is considered for the minimization task. The augmented Lagrangian particle swarm optimizer is employed, and solely the CC subdomain is re-meshed on each objective function evaluation. Numerical simulations are performed on an industrial case which is used to validate the numerical model. The results of this work exhibit not only the reduction of the cycle time achieved by the carbon fiber-charged insert with respect to a non-charged material, but also a marked improvement in the temperature homogeneity of the part obtained by the optimized CC layout. Moreover, good convergence rates of the optimization process are obtained proving that the methodology is suitable to be used in the design of complex IM inserts. Insights of the heat transfer limitations encountered by the composite tool with respect to a steel-made conventional one are given as well.

**KEYWORDS:** Transient heat transfer, Injection molding process, Overset FEM, Optimization, Cooling channels.

## 1. INTRODUCTION AND MOTIVATION

The plastic injection molding (IM) process is a cyclic manufacturing procedure that mainly consists of three defined stages: the injection and packing of the melted polymer into the mold cavity, the cooling of the plastic until reaching the ejection temperature, and, consequently, the ejection stage in which the part is ejected from the mold. Such a process is widely adopted in the manufacturing industry to make plastic parts and is perfectly suited to produce large series of products owing to the cost of conventional steel molds. The high costs and slow manufacture of these molds are mainly due to the multiple machining

*Corresponding Author: bruno.storti@univ-nantes.fr

processes involved in their fabrication, such as drilling, milling, etc. Due to the changing industry from mass production to a customer-driven perspective, and the necessity of enterprises for constant re-engineering and rapid development of new products, injection mold manufacturers are demanded for fast manufactured molds at low prices to cope with small batches of products. In this context, Additive Manufacturing (AM) has emerged as a matured technology that enables the production of polymer-based molds with complex geometries at a low cost while reducing the manufacture time.

The concept of IM process performed by plastic molds is very appealing since it combines the advantages of both technologies: the versatility of AM, with the high production rate obtained by the IM process. Nevertheless, the thermal diffusivity of such polymer-based molds is very low ($\sim 10^{-7}$ [m$^2$/s]) compared to that of steel inserts ($\sim 10^{-5}$ [m$^2$/s]), resulting in a poor thermal performance which directly impacts in the process cycle time, mold working temperature and final quality of the product. In fact, the high working temperature of such molds is identified in the literature as the main cause of their early failure [1, 2, 3, 4], preventing their wide adoption in the manufacturing industry. One goal of this work is to numerically study temperature control measures of the insert such as the usage of cooling channels (CCs), the improvement of thermal properties of the mold material, and modification of process parameters, in order to improve the performance of the overall thermal process [5].

Early experimental studies were conducted by Rahmati and Dickens [6] on a polymeric mold manufactured by the stereolithography (SLA) methodology which was able to produce a small batch of 500 parts. Due to the low thermal conductivity of the material, it was needed to significantly increase the cycle times to maintain a proper temperature of the mold while avoiding the warpage of the injected part. Mendible *et al.* [7] performed a comprehensive numerical and experimental study comparing the thermomechanical performances of rapid and conventional tooling used for plastics IM. The inserts were cooled indirectly by CC placed in the steel mold plates in contact with the inserts. The plastic insert was able to produce 116 parts before catastrophic failure. The cooling, holding and ejection times needed to be increased as well to reach the part ejection temperature. Further, the polymeric insert presented the greatest variance in shrinkage and the highest temperature differences in the molded part. A similar comparative study was conducted by Bogaerts *et al.* [2] where it was concluded that the temperature concentrations and large temperature variations were the main cause of insert failures. Furthermore, they showed that numerical models can help in both: the design of plastic inserts, and optimizing the process parameters to enhance the insert's thermal performance.

Based on the above, this article starts by comparing numerically the thermal performance of a plastic insert made of polycarbonate (PC) reinforced with carbon fibers (CF), to those obtained by steel and non-charged PC inserts. Afterwards, a novel methodology based on overset meshes [8] in the finite element method (FEM) context is proposed to optimize the CCs layout within the composite insert. Hence, this work is structured as follows. In Section 2 the study case of the production of an actual ABS part manufactured by IM is introduced, where the mold temperature is controlled by CCs. In Section 3 the governing equations along with the numerical model are presented and FEM simulations results of the steel and polymeric inserts are depicted as well. In Section 4 the overset-based FEM scheme is introduced, which is coupled with the augmented Lagrangian particle swarm optimizer (ALPSO) implemented in the open-source code pyOpt, to optimize the arrangement of the CCs within the plastic insert. In Section 5 the optimization results are presented and discussed. Finally, the conclusions and future work are presented in Section 6.

## 2. CASE OF STUDY

This section introduces a multi-plate mold given by the partners of the project which is employed in the manufacture of an automobile plastic part, and is used here for the numerical analysis and the optimization strategy. The mold possesses a single cavity to inject the melted polymer, and it is shown in Fig. 1. The fixed and mobile parts of the mold are conformed by the cover and ejector blocks, which are in contact

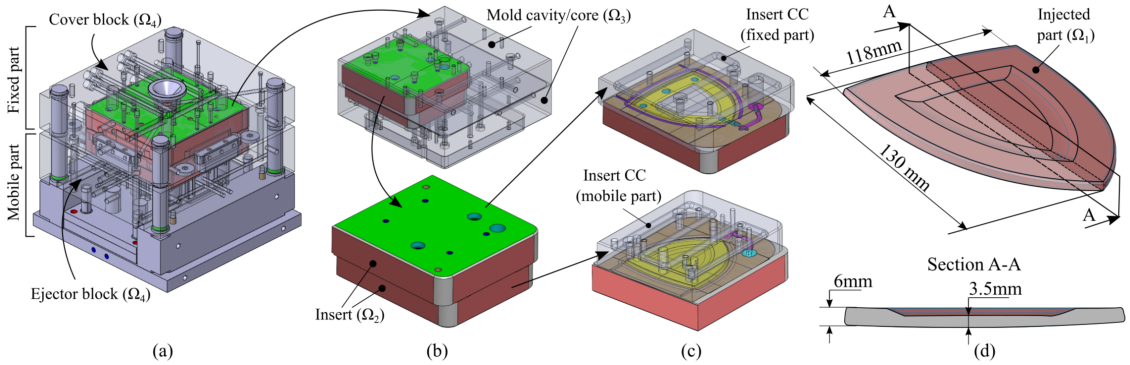


**Fig. 1** The multi-plate mold: (a) semi-transparent blocks and the molds in green, (b) the insert (bottom) and semi-transparents molds (top), (c) fixed/mobile parts of the insert showing the CCs, (d) injected part.

with the cavity and core molds. Inside the cavity and core molds are found the parts of the actual steel insert (SI) that is aiming to be replaced by a 3D-printed plastic one (PI). Straight CCs are drilled at the interior of the blocks and molds to control their temperatures. Furthermore, it can be observed from Fig. 1(c) the CCs of the insert following a conformal configuration. Such CCs were specifically designed by the mold manufacturers in order for the SI to cool down the injected polymer as quickly and homogeneously as possible. The CCs' diameter is 9mm and their distance to the cavity surface is roughly 21mm. The aforementioned configuration is employed as a reference in this work.

The part to be manufactured is made of ELIX Acrylonitrile Butadiene Styrene (ABS) P2MC, which is an amorphous material widely used in the automotive industry. The part dimensions and shape are shown in Fig. 1(d). The relatively large dimensions of the part (compared to those usually manufactured by soft tooling) and its non-constant thickness make it interesting to be addressed in this communication.

## 3. GOVERNING EQUATIONS AND NUMERICAL MODEL

**3.1 Three-Dimensional Transient Heat Conduction Problem.** Previous to tackling the optimization problem, the overall thermal performance of the conventional SI is compared to that of a PI made of PC reinforced with 10% (mass portion) of CF (PC10%CF) by performing a comprehensive 3-D FEM transient study. Similarly to [9], the most important components of the entire mold were considered, and very specific features like screws and holes were disregarded from the model. Then, four domains are studied by numerical analysis: the blocks ($\Omega_4$), the molds ($\Omega_3$), the insert ($\Omega_2$), and the injected part ($\Omega_1$) (see Figs. 1 and 2). The governing equations are those of the 3-D transient heat conduction equation, defined as:

$$\rho_1 Cp_1 \frac{\partial T_1}{\partial t} = \nabla \cdot (\kappa_1 \nabla T_1) \quad \forall T_1 \in \Omega_1 \times (0, t_f] \tag{1}$$

where $\rho_1$, $Cp_1$, $\kappa_1$ are the density, heat capacity, and thermal conductivity of the injected polymer domain $\Omega_1$, and $t_f$ the cooling time, and

$$\rho_i Cp_i \frac{\partial T_i}{\partial t} = \nabla \cdot (\kappa_i \nabla T_i) \quad \forall T_i \in \Omega_i \times (0, t_c] \quad \text{for } i = 2,3,4 \tag{2}$$

where $\rho_i$, $Cp_i$ and $\kappa_i$ are the density, heat capacity and thermal conductivity of a domain $\Omega_i$, and $t_c$ is the total cycle time. The aforementioned equations are subject to the following boundary conditions (BCs) between the injected polymer ($\Omega_1$) and the insert ($\Omega_2$) at their interfaces:

$$-\kappa_1 \frac{\partial T_1}{\partial n} = \frac{T_1 - T_2}{TCR_{1-2}} \quad \text{at} \quad \Gamma_{1-2} \quad \forall t \in [0, t_f] \tag{3}$$

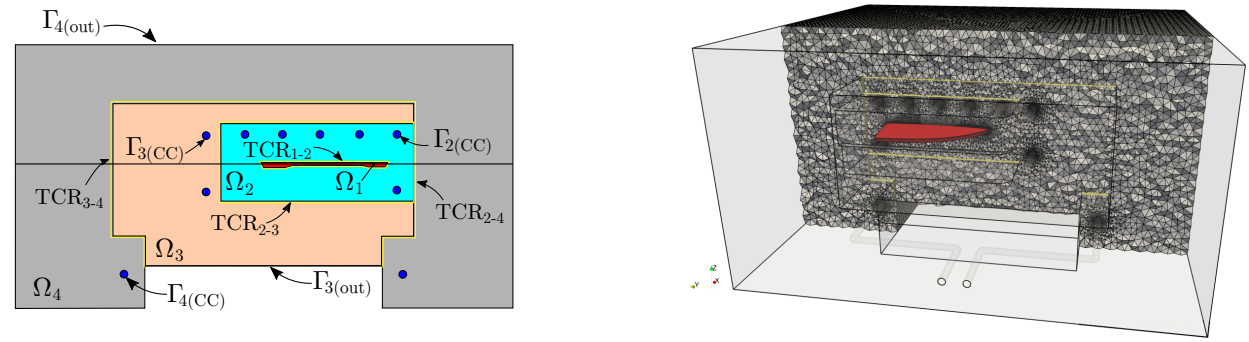


(a) Scheme of computational domains and interfaces.

(b) Conformal unstructured mesh.

**Fig. 2** Computational domains and the unstructured mesh employed for the numerical analyses.

$$-\kappa_2 \frac{\partial T_2}{\partial n} = \begin{cases} \dfrac{T_2 - T_1}{TCR_{1-2}} \text{ at } \Gamma_{1-2} \ \forall t \in [0, t_f] \\ h_{eq}(T_2 - T_{env}), \text{ at } \Gamma_{1-2} \ \forall t \in (t_f, t_c] \end{cases} \tag{4}$$

where $TCR_{1-2}$ stands for the thermal contact resistance between the polymer and the insert, and $h_{eq}$ and $T_{env}$ are the heat transfer coefficient between the molds and the environment, and the ambient temperature, respectively. Both convective and radiative effects are considered in $h_{eq}$ [10]. The first and second line of Eqn. (4) models the cooling and ejection stages, respectively. Regarding the non-perfect contact considered here between the different molds, the heat flux at the interface $\Gamma_{i-j}$ of a mold $\Omega_i$ in contact with a mold $\Omega_j$ is modeled as:

$$-\kappa_i \frac{\partial T_i}{\partial n} = \frac{T_i - T_j}{TCR_{i-j}} \quad \text{at} \quad \Gamma_{i-j} \ \forall t \in [0, t_c], \quad \text{for} \quad i, j = 2,3,4 \wedge i \neq j \tag{5}$$

where $TCR_{i-j}$ is the TCR considered at their interfaces. Furthermore, the heat flux exchanged by the molds with the environment through external surfaces is modeled as follows:

$$-\kappa_i \frac{\partial T_i}{\partial n} = h_{eq}(T_i - T_{env}) \quad \text{at} \quad \Gamma_{i(out)} \forall t \in [0, t_c] \quad \text{for} \quad i = 3,4 \tag{6}$$

where $\Gamma_{i(out)}$ is the surface of a given mold $\Omega_i$ in contact with the surrounding air (only apply for $\Omega_3$ and $\Omega_4$ domains, see Fig. 2a). The heat transfer between the molds and the CCs is modeled as:

$$-\kappa_i \frac{\partial T_i}{\partial n} = h_c(T_i - T_c) \quad \text{at} \quad \Gamma_{i(CC)} \forall t \in [0, t_c] \quad \text{for} \quad i = 2,3,4 \tag{7}$$

where $h_c$ is the heat transfer coefficient between the mold and the coolant, and $T_c$ stands for the temperature of the coolant fluid. Due to the non-steady thermal behavior of the injection process [10], the initial condition $T_1\left(t = 0^+\right) = T_{inj}$ is applied to the part domain $\Omega_1$ at the beginning of each injection cycle ($t = 0^+$), being $T_{inj}$ the injection temperature of the melted polymer, and the condition $T_i\left(t = 0^+\right) = T_i\left(t = t_c^-\right)$ is applied in the molds $\Omega_i$ for $i = 2,3,4$, where the temperature field at $t = 0^+$ is obtained from the result at the end of the previous injection cycle $t = t_c^-$. The PETSc-FEM software is employed to solve the equations on a unstructured mesh of roughly 6.4 Millions tetrahedral linear elements (see Fig.2b) which was adopted from a convergence study.

**3.2 Material Properties and Process Parameters.** The thermal and material properties employed for the block, mold, steel insert, and injected polymer are depicted in Table 1. Such values were obtained from the datasheets given by the mold manufacturer. The thermal properties measurements of the PC10%CF

material were performed on samples of $15 \times 15 \times 3[\text{mm}^3]$ manufactured by partners of the project with a 3D printer Lynxter S600D. The thermal conductivity measurement was performed at the laboratories of LTEN at Polytech, University of Nantes, by using an in-house device based on the guarded hot plate principle, at increasing temperatures from 40[°C] until 120[°C]. Negligible variations of the thermal conductivity were observed at the different temperatures. The experimentally measured thermal conductivity is subject to uncertainties primarily arising from variations in sample thickness measurements and the accuracy and stability of temperature measurements obtained by the device thermocouples used to compute the heat flux through the sample. The TCR between the sample and the hot/cold plates, along with losses resulting from non-ideal insulation, can further impact the thermocouples data. However, such effects were mitigated in this study through the use of conductive grease and an insulating guard. The composition of the composite samples also introduces uncertainty in the thermal conductivity measurement. The cumulative uncertainty associated with the in-house machine, which includes thickness and heat flow measurements, is estimated to be ±2.50%. The standard deviation of thermal conductivity, based on measurements of two printed PC10%CF samples, was ±1.30%. By combining the uncertainties related to the experimental device and the obtained measurements, the overall uncertainty for the reported conductivity value in Table 1 was determined to be ±2.81% (±0.009 [W/(mK)]).

The measurement of the specific heat of PC10%CF was performed at the laboratory as well by employing the Differential Scanning Calorimetry (DSC) Q200 device. The material was studied in the range from 20[°C] to 280[°C] with single heating, at a heating rate of 10[°C/min] on a 35[mg] sample. The $C_p$ value at 100[°C] was considered for the simulations. The primary sources of uncertainty associated with the DSC measurements are attributed to the instrument calibration, sample preparation, encompassing the homogeneity, purity, and mass of the specimen, baseline correction, utilized for the acquisition of the net heat flow, and measurement conditions that comprised the heating rate, pressure, and atmosphere. After proper calibration with an indium sample and a normalize procedure, the DSC Q200 device is capable of achieving an incertitude of roughly ±1.70% in the $C_p$ measurements [11]. The uncertainties concerning sample preparation, baseline correction, and measurement conditions were estimated by performing measurements with the DSC Q200 device on four PC10%CF samples, where the standard deviation was computed in ±4.97%. The pairs of aluminum crucibles and lids employed for the reference and sample were weighted on each measurement so as to have a weight difference below 0.05 [mg] to minimize heat flux measurement uncertainties. Then, the combined uncertainty of the $C_p$ measurement reported in Table 1 resulted in ±5.25% (±70.82[J/(kgK)]). Regarding the main IM process parameters, they are depicted in Table 2. The convective heat transfer

**Table 1** Material and thermal properties of the injected polymer, insert, and molds.

| | Injected polymer $\Omega_1$ | Insert $\Omega_2$ | | Mold $\Omega_3$ | Block $\Omega_4$ |
|---|---|---|---|---|---|
| Material | ABS | AISI P20+S | PC%10CF | AISI P20 | AISI 1045 |
| $\rho$[kg/(m$^3$)] | 1030 | 7840 | 1137 | 7840 | 7870 |
| $C_p$[J/(kgK)] | 1800 | 470 | 1349 | 470 | 486 |
| $\kappa$[W/(mK)] | 0.2 | 39.8 | 0.33 | 32.5 | 44.9 |

coefficient $h_c$ was computed by considering the Nusselt number obtained by the Dittus-Boelter correlation for fully developed fluids [12].

**3.3 Handling of Thermal Contact Resistances.** Due to the consideration of non-perfect contacts at the domain-domain interfaces, an algorithm was developed in the framework of this work to automatically duplicate the nodes at the boundaries to solve for the temperature at each contact surface. Contrary to [9], a conformal approach was followed here. Therefore, the notation $\Gamma_{i-j(\Omega_i)}$ is used henceforth to refer to the $\Omega_i - \Omega_j$ contact surfaces, on the $\Omega_i$ side. An exhaustive review of the literature was conducted in this work

**Table 2** Main process parameters employed for the study case.

| Main process temperatures | | | Heat transfer coefficients | | Process times | |
|---|---|---|---|---|---|---|
| $T_{inj}$[°C] | $T_c$[°C] | $T_{env}$[°C] | $h_{eq}$[W/(m$^2$K)] | $h_c$[W/(m$^2$K)] | $t_f$[s] | $t_c$[s] |
| 240 | 65 | 20 | 10 | 10100 | 37 | 46 |

to identify the TCR values. For the mold-block ($\Gamma_{3-4}$), SI-mold ($\Gamma_{2-4}$), and SI-block ($\Gamma_{2-3}$) interfaces the TCRs were determined based on the investigations of Cheng et al. [9], where a thermal conductance (reciprocal of the TCR) of 30000[W/(m$^2$K)] was numerically determined and experimentally validated. The TCR at the PI-mold and PI-block interfaces was obtained from the experimental investigation of Fuller et al. [13], which indicates that the thermal conductance remains roughly constant ($\approx$ 165[W/(m$^2$K)]) for a metal-PC solid interface with a sufficiently high contact pressure (>800[kPa]). The TCR at the injected polymer-SI ($\Gamma_{1-2}$) interface is derived from the experimental data of Pignon et al. [14], which examine the injection of ABS into a steel mold cavity. In the absence of literature on the precise characterization of the TCR between PI molds and melted polymers in the IM context, the value was obtained based on the recent experimental work of Le Mouellic et al. [15], which identified TCR values at a polymer-polymer interface during an overmolding process. Based on the above, the adopted values are summarized in Table 3.

**Table 3** Thermal contact resistances (values in [m$^2$K/(W)]) defined at the domain-domain interfaces.

| | $TCR_{1-2}$ | $TCR_{2-3}$ | $TCR_{2-4}$ | $TCR_{3-4}$ |
|---|---|---|---|---|
| Steel insert case | $1\times10^{-3}$ | $3.33\times10^{-5}$ | $3.33\times10^{-5}$ | $3.33\times10^{-5}$ |
| Plastic insert case | $1\times10^{-2}$ | $6\times10^{-3}$ | $6\times10^{-3}$ | $3.33\times10^{-5}$ |

**3.4 Steel and Plastic Inserts Comparison.** The main results of the 3-D transient heat transfer simulations are presented in Fig. 3a and Table 4 (default configurations). The part and cavity surfaces results correspond to $\Gamma_{1-2(\Omega_1)}$ and $\Gamma_{1-2(\Omega_2)}$ interfaces, respectively. The SI quickly reached the periodic steady state (PSS) in 4 cycles, and the mean temperature at the part surface at the end of the cooling stage is 0.1[°C] difference with the ejection temperature ($T_e$) required by the provider of the ABS material (75[°C]), validating our numerical model and enabling us to use the SI case as a reference point. Furthermore, the mean temperature of the melted polymer ($\bar{T}_{\Omega_1}$) at the end of the cooling stage is 95.7[°C], being below the glass transition temperature (Tg) of ABS, which is $\approx$ 105[°C], required to eject the part. On the other hand,

**Table 4** Mean temperatures obtained by SI and PI cases at the end of the cooling (once reached the PSS).

| | Material | $L_{P-CC}$[mm] | $t_f$[s] | $t_c$[s] | $\bar{T}_{\Gamma_{1-2(\Omega_1)}}$[°C] | $\bar{T}_{\Gamma_{1-2(\Omega_2)}}$[°C] | $\bar{T}_{\Omega_1}$[°C] |
|---|---|---|---|---|---|---|---|
| Default IM parameters/configuration of CCs | | | | | | | |
| SI: default | AISI P20+S | 21 | 37 | 46 | 74.90 | 70.02 | 95.7 |
| PI: default | PC %10 CF | 21 | 37 | 46 | 197.6 | 175.57 | 208.13 |
| Modified IM parameters/configuration of CCs | | | | | | | |
| PI: case 1 | PC %10 CF | 21 | 360 | 420 | 75.36 | 72.06 | 77.69 |
| PI: case 2 | PC %10 CF | 9 | 240 | 300 | 75.95 | 69.21 | 80.40 |
| PI: case 3 | PC (non-charged) | 21 | 540 | 600 | 75.23 | 73.30 | 78.81 |

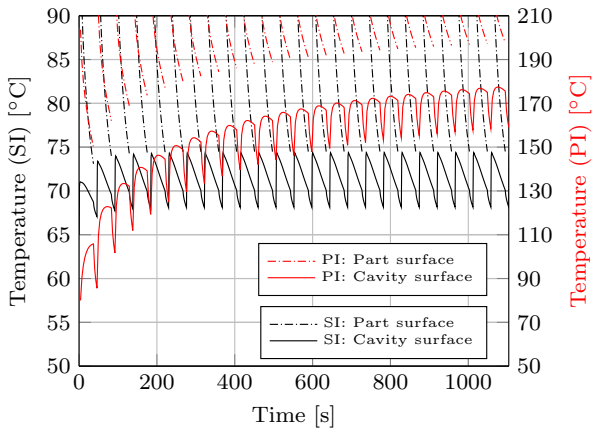


(a) Steel and plastic inserts cases: default IM parameters.

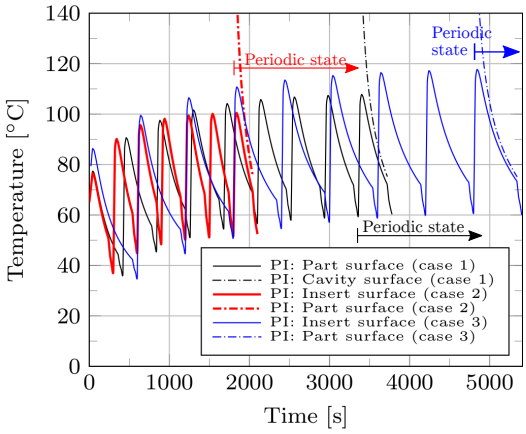


(b) Plastic insert cases: modified IM parameters.

**Fig. 3** Mean temperatures at the part and cavity surfaces obtained by the SI and the PI.

for the same IM parameters, the PI took roughly 19 cycles to reach the PSS; however, the temperature of the part at the end of the cooling stage is as high as 197.6 [°C], making it impossible to eject the part. It is important to clarify that when taking into account the uncertainties associated with $\kappa$ and $C_p$ measurements obtained from the experimental devices in Section 3.2, i.e., by considering the maximum and minimum thermal diffusivity values, the numerical simulations presented in Fig. 3a (PI) yielded maximum differences of $\pm 0.75$[°C] and $\pm 0.44$[°C] for the cavity surface and part surface mean temperatures, respectively. It can be further observed from Fig. 3a that $\bar{T}_{\Gamma_{1-2(\Omega_2)}}$ reaches values above the Tg of the material, which is approximately 147 [°C] for the PC polymer. Hence, modified IM parameters and CCs configurations are addressed next.

**3.5 Injection Process Parameters and Thermal Conductivity Sensibility.** To achieve the $T_e$ of the part for the PI, the IM parameters such as $t_f$, $t_e$, and $T_c$ have to be modified. If nothing is specified, the following values are considered henceforth: $T_c = 10$[°C] and $t_e = 60$[s]. Then, the $t_f$ to achieve $\bar{T}_{\Gamma_{1-2(\Omega_1)}} \leq T_e \pm 1$[°C] is numerically assessed in two cases for the PC%10CF insert by changing the distance between CCs and part surfaces ($L_{P-CC}$). Further, such time is also evaluated when considering a PC material without CF charges. For the non-charged PC insert, the following properties were considered: $\kappa = 0.21$[W/(mK)], $C_p = 1300$[J/(kgK)], and $\rho = 1210$[kg/(m$^3$)]. Both the cases and the results are depicted in Table 4 and Fig. 3b. It can be seen from Fig. 3b that to reach the $T_e$ in the PSS, 6 injection cycles are required for case 2, while 8 cycles are required for cases 1 and 3. Results also show the sensibility of the cycle times to the insert thermal conductivity. While $t_c = 600$[s] is required for the non-charged PC insert, such a time is reduced to $t_c = 420$[s] for the PC10%CF insert, representing a 30% reduction of the cycle time. Further reduction of $t_c$ is obtained by decreasing the distance $L_{P-CC}$ to one diameter distance (9[mm]) in case 2; however, as will be addressed in the following sections, the temperature homogeneity at the part surface is affected by such an arrangement, and, hence, an optimization strategy is introduced next.

## 4. OPTIMIZATION OF COOLING CHANNELS LAYOUT

**4.1 Detailed Model.** The employment of a detailed model of this work consists on solving the transient heat equations on the domains $\Omega_1$ and $\Omega_2$ solely, with the precaution of considering the temperature field obtained by the 3D full model at the interface boundary $\Gamma_{2-3(\Omega_3)}$ as BC of $\Omega_2$ . Then, the equations to be solved by the detailed model are those of Section (3), but considering as the BC of Eqn. (5) the stationary

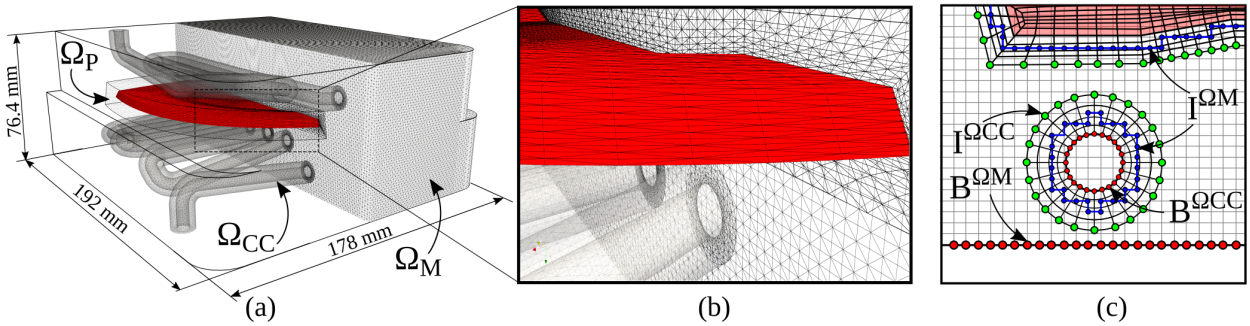


**Fig. 4** Structured grids (a), and a detailed view, (b) used by the overset scheme. Nodes grouping in sets (c).

temperature field of $\Gamma_{2-3(\Omega_3)}$. It is worth mentioning that the Dittus-Boelter correlation is also employed here due to a roughly uniform cooling temperature estimation and a constant flow regime assumption. Nonetheless, the methodology introduced in the subsequent sections can be readily extended to disregard the aforementioned correlation by incorporating a conjugated heat transfer (CHT) approach at the CCs-insert interface. Specifically, by employing the adv-diff module of PETScFEM, the advection-diffusion equations can be solved within the CCs assuming a fixed velocity field. For a more precise simulation, the velocities and pressure fields of the coolant can be additionally solved using the Navier-Stokes module. The decision to use a CHT condition should be made by considering the trade-off between the additional computational cost and the increased accuracy it offers in the specific case at hand.

**4.2 Overset-FEM Methodology.** The overset-FEM scheme proposed here is based on decomposing the computational domain $\Omega = \Omega_1 \cup \Omega_2$, on three easy-to-mesh domains accounting for the injected part $\Omega_P$, the insert $\Omega_M$, and the CCs geometry $\Omega_{CC}$ (see Fig. 4a). This decomposition allows, on the one hand, generating anisotropically refined high-quality structured meshes to properly capture high thermal gradients and material changing properties at the interfaces (see Fig. 4b), and, on the other hand, avoiding remeshing the entire computational domain on each objective function (OF) evaluation, since only the CCs domain would be required to re-mesh. The $\Omega_M$, $\Omega_P$, and $\Omega_{CC}$ meshes are conformed by 5.27 million, 0.45 million, and 2.6-3.9 million elements, respectively. The amount of elements of $\Omega_{CC}$ varies according to the shape and length of the CCs proposed by the optimizer.

*Nodes grouping in sets.* To follow an overset-scheme strategy, the nodes of each domain must be split into groups according to their location or functionalities [12]. In this way, three sets of nodes are encountered for each domain: set **B** which are the nodes where the boundaries condition are defined, set **I** being the nodes in charge of transferring the information between domains through interpolation, and set **Z** the interior nodes and are the unknowns of each system of equations (remaining nodes). A 2-D scheme is shown in Fig. 4c.

*Algebraic systems in the overset context.* Due to the nodes-splitting of each domain, the algebraic systems are split as well. Let us consider the algebraic form of Eqn. (2) which, after applying a FEM discretization and employing the Galerkin formulation, yields:

$$\mathbf{C}\dot{\mathbf{T}} + \mathbf{K}\mathbf{T} = \mathbf{Q} \tag{8}$$

being **C**, **K** and **Q** the global capacitance matrix, conduction matrix and heat load vector, respectively. Then, by employing the unconditionally stable implicit backward euler scheme to integrate Eqn. (8), and

by splitting the algebraic system by the nodes grouping, we obtain:

$$\left(\frac{1}{\Delta t}\begin{bmatrix}\mathbf{C}_{BB}\mathbf{C}_{BZ}\mathbf{C}_{BI}\\ \mathbf{C}_{ZB}\mathbf{C}_{ZZ}\mathbf{C}_{ZI}\\ \mathbf{C}_{IB}\,\mathbf{C}_{IZ}\,\mathbf{C}_{II}\end{bmatrix}+\begin{bmatrix}\mathbf{K}_{BB}\mathbf{K}_{BZ}\mathbf{K}_{BI}\\ \mathbf{K}_{ZB}\mathbf{K}_{ZZ}\mathbf{K}_{ZI}\\ \mathbf{K}_{IB}\,\mathbf{K}_{IZ}\,\mathbf{K}_{II}\end{bmatrix}\right)\begin{bmatrix}\mathbf{T}_B\\ \mathbf{T}_Z\\ \mathbf{T}_I\end{bmatrix}^{t+\Delta t}=\begin{bmatrix}\mathbf{Q}_B\\ \mathbf{Q}_Z\\ \mathbf{Q}_I\end{bmatrix}+\left(\frac{1}{\Delta t}\begin{bmatrix}\mathbf{C}_{BB}\mathbf{C}_{BZ}\mathbf{C}_{BI}\\ \mathbf{C}_{ZB}\mathbf{C}_{ZZ}\mathbf{C}_{ZI}\\ \mathbf{C}_{IB}\,\mathbf{C}_{IZ}\,\mathbf{C}_{II}\end{bmatrix}\right)\begin{bmatrix}\mathbf{T}_B\\ \mathbf{T}_Z\\ \mathbf{T}_I\end{bmatrix}^{t} \tag{9}$$

The temperature values $\mathbf{T}_B^{t+\Delta t}$ will be given by the corresponding BCs, $\mathbf{T}_Z^{t+\Delta t}$ stands for the unknown temperatures, and $\mathbf{T}_I^{t+\Delta t}$ are to be interpolated from the corresponding overlapped domain. Assuming that Eqn. (9) is to be solved in $\Omega_M$, and the coupling with the $\Omega_{CC}$ is considered, then we obtain the following expression for the interior values $\mathbf{T}_Z^{(\Omega_M,t+\Delta t)}$:

$$\begin{aligned}\left(\frac{1}{\Delta t}\,\mathbf{C}_{ZZ}^{(\Omega_M,t+\Delta t)}+\mathbf{K}_{ZZ}^{(\Omega_M,t+\Delta t)}\right)\mathbf{T}_Z^{(\Omega_M,t+\Delta t)}&=\mathbf{Q}_Z+\frac{1}{\Delta t}\left(\mathbf{C}_{ZB}^{(\Omega_M,t)}\mathbf{T}_B^{(\Omega_M,t)}+\mathbf{C}_{ZZ}^{(\Omega_M,t)}\mathbf{T}_Z^{(\Omega_M,t)}+\mathbf{C}_{ZI}^{(\Omega_M,t)}\mathbf{T}_I^{(\Omega_M,t)}\right)\\&-\frac{1}{\Delta t}\left(\mathbf{C}_{ZB}^{(\Omega_M,t+\Delta t)}\mathbf{T}_B^{(\Omega_M,t+\Delta t)}+\mathbf{C}_{ZI}^{(\Omega_M,t+\Delta t)}\Pi_{CC\to M}\mathbf{T}_Z^{(\Omega_{CC},t+\Delta t)}\right)\end{aligned} \tag{10}$$

where supra-indexes indicate the corresponding domain, and $\Pi_{CC\to M}$ is a projection operator which interpolates the values from the interior nodes of $\Omega_{CC}$ to the interpolation nodes of $\Omega_M$. The domains coupling is performed in PETSc-FEM, an open-source FEM code, where a high–order interpolation is employed to preserve the accuracy and second–order convergence of the FEM solution [8].

**4.3 Optimization Problem Formulation.** The mathematical definition of the optimization problem proposed in this work is as follows:

$$\begin{aligned}\min_{\mathbf{x}}\quad & F_{obj}(\mathbf{x})\\ \text{subject to}\quad & x_{i_L}\le x_i\le x_{i_U},\quad \text{for}\quad i=1,...,n\\ & g_j(\mathbf{x})=c_{min}-c_j\le 0,\quad \text{for}\quad j=1,...,m_e\\ & h(\mathbf{x})=\overline{T}_{\Gamma_P}-\overline{T}_{\Gamma_{P(SI)}}\le 0\\ & l(\mathbf{x})=\overline{T}_{\Omega_P}-\overline{T}_{\Omega_{P(SI)}}\le 0\end{aligned} \tag{11}$$

where $F_{obj}$ is the OF to minimize, $x_{i_L}$ and $x_{i_U}$ are the lower and upper limits of the variables, $g(\mathbf{x})$ is defined to avoid superposition between CCs, and $h(\mathbf{x})$ and $l(\mathbf{x})$ are defined to achieve the ejection temperatures at the part surface ($\Gamma_P\equiv\Gamma_{1-2(\Omega_1)}$) and within the part ($\Omega_P\equiv\Omega_1$). The values of $\overline{T}_{\Gamma_P}$ and $\overline{T}_{\Omega_P}$ obtained by the SI case (see Table 4) are used for the constraints. Similarly to [10], the OF to be minimized is conformed of two terms, one aiming to improve the temperature homogeneity at the part surface, and the other intended to reduce its thermal gap between maximum and minimum temperatures. Then the OF yields:

$$F_{obj}(\mathbf{x})=w\,\frac{\left[\int_{\Gamma_P}\left(\bar{T}(\mathbf{x},t_f)-T(\mathbf{x},t_f)\right)^2 d\Gamma_P\right]}{F_{10}}+(1-w)\,\frac{T_{\Gamma_P}^{max}(\mathbf{x},t_f)-T_{\Gamma_P}^{min}(\mathbf{x},t_f)}{F_{20}} \tag{12}$$

where $T_{\Gamma_P}^{max}$ and $T_{\Gamma_P}^{min}$ are the maximum and minimum values of the temperature at the part surface, $F_{10}$ and $F_{20}$ are normalization parameters, and $\omega$ is a weighting parameter. Values obtained by the PI: case 2 (see Table 4) are used for normalization. The layout of the CCs at the fixed and mobile parts of the insert is defined by a total of 23 variables (see Fig. 5) that define the proximity of the CCs to the cavity surface and the distances between the branches of the serial CCs. Then, the design variables are defined in $\mathbf{x}$ as:

$$\mathbf{x}=\Big\{\underbrace{z_1,\,z_2,\,...,\,z_6,\,d_1,\,d_2}_{\textbf{Mobile part}},\,\underbrace{z_7,\,z_8,\,...,\,z_{16},\,d_3,\,d_4,\,d_5,\,d_6,\,d_7}_{\textbf{Fixed part}}\Big\} \tag{13}$$

Since the part geometry is symmetric with respect to the plane $y-z$, the design variables define one-half of the CCs (red points in Fig. 5) and the other half is achieved by symmetry (gray points). One main novelty of this approach is that the CCs are allowed to automatically bend at their mid-length.

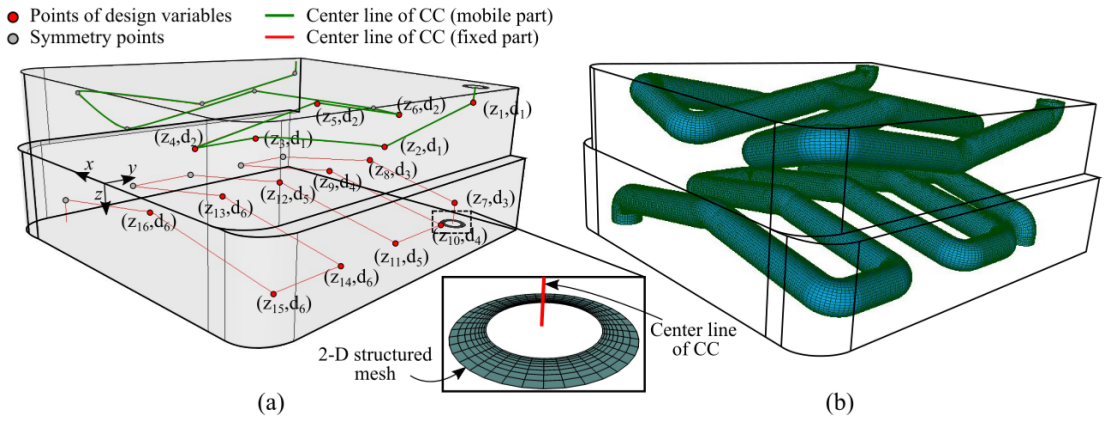


**Fig. 5** Design variables employed to define the CCs center lines (a), and the 3-D mesh of $\Omega_{CC}$ (b) obtained by extruding a 2-D structured mesh (detailed view) through such lines. The CCs can bend at their mid-length.

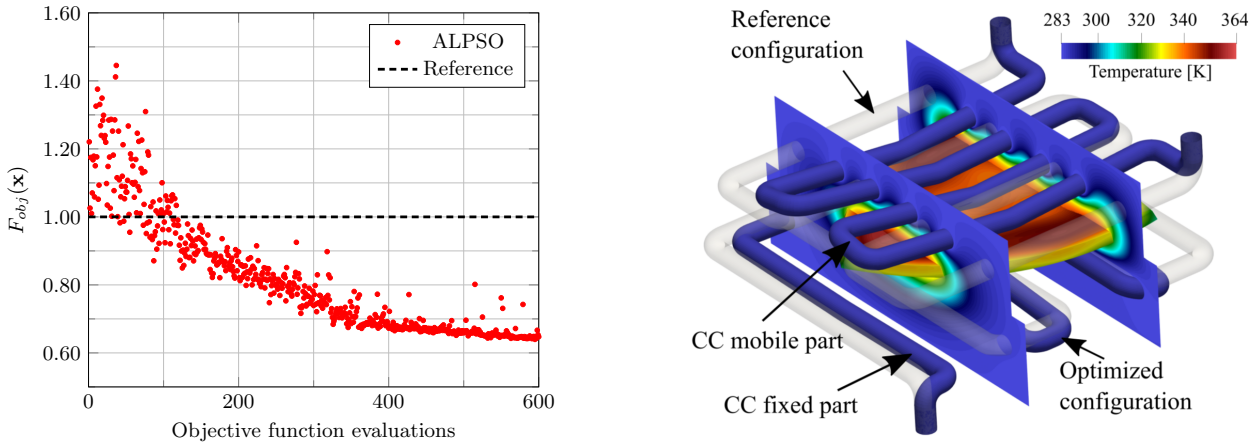


(a) Convergence rate of ALPSO

(b) Temperature field obtained by the optimized CCs

**Fig. 6** Results of the optimization process obtained by the overset-FEM methodology.

## 5. OPTIMIZATION RESULTS AND DISCUSSION

The optimization procedure was stopped after performing 600 OF evaluations of the ALPSO. Since each OF evaluation involved the transient simulations of between 6-8 injection cycles, the computing time of each was roughly 8 hours on a single core. The optimization process was parallelized on 40 cores of the High-Performance Computer cluster of Pays de la Loire by employing the DPM capabilities of pyOpt, where each swarm particle is computed on each core. The total optimization procedure took approximately 5 days. As can be seen in Fig. 6a, a very clear convergence of the OF was obtained by the proposed optimization methodology. An improvement of 35% of the OF value was finally obtained (see also Table 5).

The optimized CCs layout is shown in Fig. 6b, where it is observed that the distances between branches are greatly reduced with respect to those of the reference configuration. Since regions of the injected polymer with high surface-to-volume ratios, such as borders and corners, cool down faster than others with lower ratios, no CCs are needed in such areas. Furthermore, the CCs tend to get closer to the part near its center; however, the opposite occurs at the sharp corners where CCs tend to go further from the surface. In Table 5 are summarized the values obtained at the end of the cooling stage (once reached the PSS) for the optimized case, the case 2 of Table 4 used as reference, and the SI case for comparison purposes. Results show a reduction of 42% of the temperature deviation term $T_{\Gamma_p}^{dev}$ (numerator of first term of Eqn. (12)), and a

**Table 5** Results obtained by the optimized CCs compared to reference cases.

| | $t_f$[s] / $t_c$[s] | $\bar{T}_{\Gamma_P}$[°C] | $T_{\Gamma_P}^{dev}$ | $T_{\Gamma_P}^{max}$[°C] | $T_{\Gamma_P}^{min}$[°C] | $\Delta T_{\Gamma_P}$[°C] | $\bar{T}_{\Omega_P}$[°C] |
|---|---|---|---|---|---|---|---|
| Steel insert case | 37/46 | 74.90 | 0.13 | 66.27 | 77.51 | 11.24 | 95.7 |
| Reference (PI: case 2) | 240/300 | 75.95 | 2.87 | 92.44 | 39.06 | 53.38 | 80.07 |
| PI: Optimized CCs | 240/300 | 71.18 | 1.65 | 86.95 | 40.02 | 46.92 | 75.65 |

reduction of more than 6 [°C] of the term accounting for the temperature gap at the part surface $\Delta T_{\Gamma_P}$, with respect to the reference case. Furthermore, the constraints of the optimization task were accomplished, reaching a mean temperature at the part surface below $T_e$, and a mean temperature of the part volume much below the $T_g$ of the polymer. Regardless of the improvements achieved by the optimized CCs configuration in the PI, it becomes evident from the results of Table 5 that the thermal performance of such an insert in terms of cycle times, temperature homogeneity and working temperatures, is limited by its thermal conductivity, and is still far from the one obtained by the steel-made mold.

## 6. CONCLUSION AND FUTURE WORK

A comprehensive 3-D numerical study was performed to compare the thermal performance of a steel insert with cooling channels, to that of a polymer-based one. The results show the infeasibility of using such plastic inserts under the same cycle times used by steel-made ones due to their low thermal diffusivity. Further, since cycle times are very sensitive to the insert thermal conductivity, a 30% reduction can be obtained by the polycarbonate matrix charged with carbon fibers with respect to a non-charged material. A numerical optimization strategy specifically conceived for additively manufactured inserts with cooling channels was successfully implemented based on 3-D structured overlapped meshes and a stochastic algorithm. Results showed an improvement with respect to a non-optimized configuration of roughly 42% on the temperature homogeneity of the final part, and a reduction of more than 6 [°C] between maximum and minimum temperatures of the part surface for the same insert material and process parameters. The presented optimization numerical methodology has shown potential future applications for assisting mold designers in the manufacture of 3D printed inserts with specifically designed cooling channels. This approach, combined with the use of high-performance composites, has the potential to reduce cycle times and improve heat transfer within the mold, which may lead to a reduction in thermal stresses and an increase in tool life. Future work will aim to extend the methodology to consider the thermomechanical performance of the insert, as well as experimental validation of the numerical optimization results. Furthermore, this investigation highlights the pressing need for the development of new charged polymers with improved thermal conductivity to be used in 3D printed molds. The ongoing research being conducted in this work is dedicated to investigating this very issue.

## ACKNOWLEDGMENT

The authors gratefully acknowledge the financial support received from the *Banque Publique d'Investissement (BPI)* for the project *SAMFAST: Fabrication additive rapide d'empreintes d'outillages d'injection plastique*. The support given in the framework of the project by the enterprises CERO, NANOVIA, IRMA and COMPOSITIC is also gratefully acknowledged.

# REFERENCES


[1] Whatcott, T. B., *Effects of Conformal Cooling Channels on Additively Manufactured Injection Molding Tooling*, Ph.D. thesis, Brigham Young University (2020).

[2] Bogaerts, L., Faes, M., Bergen, J., Cloots, J., Vasiliauskaite, E., Vogeler, F. and Moens, D., "Influence of thermo-mechanical loads on the lifetime of plastic inserts for injection moulds produced via additive manufacturing", *Procedia CIRP*, 96, pp. 109–114 (2021).

[3] Bagalkot, A., Pons, D., Symons, D. and Clucas, D., "Categorization of failures in polymer rapid tools used for injection molding", *Processes*, 7(1), p. 17 (2019).

[4] Lozano, A. B., Álvarez, S. H., Isaza, C. V. and Montealegre-Rubio, W., "Analysis and Advances in Additive Manufacturing as a New Technology to Make Polymer Injection Molds for World-Class Production Systems", *Polymers*, 14(9), p. 1646 (2022).

[5] Schuh, G., Bergweiler, G., Lukas, G. and Oly, M., "Towards Temperature Control Measures for Polymer Additive Injection Molds", *Procedia CIRP*, 93, pp. 90–95 (2020).

[6] Rahmati, S. and Dickens, P., "Rapid tooling analysis of Stereolithography injection mould tooling", *International Journal of Machine Tools and Manufacture*, 47(5), pp. 740–747 (2007).

[7] Mendible, G. A., Rulander, J. A. and Johnston, S. P., "Comparative study of rapid and conventional tooling for plastics injection molding", *Rapid Prototyping Journal* (2017).

[8] Storti, B., Garelli, L., Storti, M. and D'Elía, J., "A matrix-free Chimera approach based on Dirichlet–Dirichlet coupling for domain composition purposes", *Computers & Mathematics with Applications*, 79(12), pp. 3310–3330 (2020).

[9] Chen, L., Zhou, X., Huang, Z. and Zhou, H., "Three-dimensional transient finite element cooling simulation for injection molding tools", *The International Journal of Advanced Manufacturing Technology*, 120(11), pp. 7919–7936 (2022).

[10] Agazzi, A., Sobotka, V., LeGoff, R. and Jarny, Y., "Optimal cooling design in injection moulding process–A new approach based on morphological surfaces", *Applied Thermal Engineering*, 52(1), pp. 170–178 (2013).

[11] Kahwaji, S., Johnson, M. B. and White, M. A., "Thermal property determination for phase change materials", *The Journal of Chemical Thermodynamics*, 160, p. 106439 (2021).

[12] Storti, B., Garelli, L., Storti, M. and D'elia, J., "Optimization of an internal blade cooling passage configuration using a Chimera approach and parallel computing", *Finite Elements in Analysis and Design*, 177, p. 103423 (2020).

[13] Fuller, J. J. and Marotta, E., "Thermal contact conductance of metal/polymer joints: an analytical and experimental investigation", *Journal of Thermophysics and Heat Transfer*, 15(2), pp. 228–238 (2001).

[14] Pignon, B., Sobotka, V., Boyard, N. and Delaunay, D., "Improvement of heat transfer analytical models for thermoplastic injection molding and comparison with experiments", *International Journal of Heat and Mass Transfer*, 118, pp. 14–26 (2018).

[15] Le Mouellic, P., Boyard, N., Bailleul, J.-L., Lefevre, N., Gaudry, T. and Veille, J.-M., "Development of an original overmoulding device to analyze heat transfer at polymer/polymer interface during overmoulding", *Applied Thermal Engineering*, p. 119042 (2022).